Turning OPM-MEG into a Wearable Technology

Natalie Rhodes[1], Niall Holmes[1], Ryan Hill[1], Gareth Barnes[2], Richard Bowtell[1], Matthew Brookes[1],[3] and Elena Boto[1],[3]

Abstract

This chapter explores the use of optically-pumped magnetometers (OPMs) as a tool for magnetoencephalography (MEG). Conventional MEG systems use superconducting quantum interference devices (SQUIDs) to measure the femto-Tesla-level magnetic fields at the head surface that are generated by synchronized (dendritic) neural current flow in the brain. SQUIDs require cryogenic cooling to maintain a low operating temperature and must be bathed in liquid helium and held in a rigid helmet with thermal insulation to protect the participant. Scanners are therefore large, cumbersome, and one-size-fits-all; movement of the participant relative to the fixed array degrades quality of data. Conversely, OPMs exploit the spin properties of alkali atoms to measure local magnetic field. They can be constructed with an external surface at close-to-body temperature, while maintaining a small, light, and flexible form. In this chapter, we show how commercial OPMs can form the basis of a MEG system that allows sensors to get closer to the scalp surface, improving signal strength and spatial specificity. Further, OPMs allow the flexibility to adapt a sensor array to any head shape or size, and even facilitate natural movement throughout MEG acquisition. We explain why OPMs are emerging as a stand-out replacement for SQUIDs, and how nascent sensor designs enable multi-axis measurements. We look at the practical requirements for designing sensor arrays that facilitate high spatial resolution imaging. We further describe how allowing movement requires additional background magnetic field suppression. Finally, we review recent literature to demonstrate how OPM-MEG has been used to enable novel neuroscientific experimentation.

---

[1] Sir Peter Mansfield Imaging Centre, School of Physics and Astronomy, University of Nottingham, University Park, Nottingham, NG7 2RD, UK

[2] Wellcome Trust Centre for NeuroImaging, University College London, London, WC1N 3BG, UK

[3] Cerca Magnetics Limited, Headcorn Road, Staplehurst, Kent, UK

Key Words: magnetoencephalography, optically-pumped magnetometers, triaxial measurement, magnetic shielding, magnetic field suppression, MEG array design

1. Introduction

Functional neuroimaging offers a non-invasive window on neural activity in the human brain. This ability to probe the formation and dissolution of brain networks in real-time, as the brain responds to cognitive demand, not only allows new ways to understand healthy brain function, but also enables us to investigate pathological activity in various disorders, ranging from neurodevelopmental problems (e.g. Autism) in the very young, to neurodegenerative disease (e.g. Alzheimer's) in the elderly. Indeed, the powerful techniques that have been made available over the last few decades have told us a great deal about the nature of human brain activity in health and disease.

Despite the successes, current neuroimaging methods are limited. Tools, such as functional magnetic resonance imaging (fMRI) (Ogawa et al., 1990) require participants to lie in a scanner and remain stationary during lengthy data acquisitions. Many cohorts, particularly patients or young people, find this environment extremely challenging. In addition, the need for immobility limits the types of experimental paradigms that can be employed; for example, any paradigm featuring natural movement of the head or body is impossible. Other techniques, such as electroencephalography (EEG) (Berger, 1929) or functional near infrared spectroscopy (fNIRS) (Hoshi and Tamura, 1993), are (theoretically) wearable but suffer from poorer performance. For example, EEG has very high sensitivity to artefacts from non-brain sources such as muscles in the head or neck, which degrade data quality, particularly during movement (Jiang et al., 2019, Boto et al., 2019). Further, both EEG and fNIRS suffer from poor spatial resolution, and fNIRS also has very poor temporal resolution since (like fMRI) it is only able to detect indirect (haemodynamic) responses to brain activity. In sum, the current landscape of functional neuroimaging methodologies is highly limited either by scanner environment or performance, and the development of technology to overcome this is important.

Magnetoencephalography (MEG) measures the magnetic fields generated by neural current flow in the brain (Cohen, 1968). This is the magnetic counterpart of EEG, which measures electrical potentials at the scalp that are generated by (mostly) the same neural current flow. Unlike EEG, where electrical potentials are distorted spatially by the high resistivity of the skull, magnetic fields pass through the skull undistorted. Consequently, spatial resolution in MEG is significantly improved compared to EEG. Further, MEG can assess brain function with less interference from non-neural sources (Muthukumaraswamy, 2013). The measured fields are very small, on the order of femtotesla (fT, 10^{-15} T) (Baillet, 2017) but nevertheless measurable via an array of *superconducting quantum interference devices* (SQUIDs). MEG represents arguably the best platform for functional neuroimaging,

providing direct access to electrophysiological responses alongside high spatial and temporal resolution imaging. However, the sensors must be housed in a rigid helmet and bathed in a dewar of liquid helium to maintain the 4 K (-269 °C) temperature required for superconductivity. This means that, like fMRI, subjects must remain still for long periods of time, and consequently, the environment is extremely challenging for some cohorts. In addition, the rigid helmet is one size fits all and built for adults. Because the magnetic field from the brain decreases with the square of the distance from the source to the sensor, this means sensitivity is limited, particularly for individuals with small heads.

In recent years, advances in non-cryogenic magnetic field sensors have led to a potential replacement for the cumbersome SQUID-based MEG systems. *Optically-pumped magnetometers* (OPMs) use the quantum mechanical properties of alkali metal atoms to create a magnetically sensitive atomic ensemble, which can be manipulated to measure very small magnetic fields. OPMs have a compact, lightweight sensor design and do not require cryogenic cooling, meaning they can be mounted directly onto, or held near, the scalp. Such wearable OPM arrays ostensibly move with the participant, allowing for comfortable naturalistic movements during scanning. In addition, because the OPMs can get closer to the head, they offer, in principle, higher sensitivity and greater flexibility to adapt to head shape and size. Consequently, OPMs, offer the promise to revolutionise MEG, providing, for the first time, a functional imaging modality with both a naturalistic environment, free movement, and high spatial and temporal resolution.

Here, we will discuss the limitations of the current generation of cryogenic MEG systems and outline how the use of OPMs alleviates many of these problems, forming the basis of next-generation MEG instrumentation. We will then describe the technical challenges surrounding the development of a wearable OPM-MEG system that enables participant movement. Finally, we will discuss the potential applications, including novel experimental paradigms involving a range of natural movements, and possible clinical avenues of research.

a. An overview of conventional MEG

The basic building block of a conventional MEG system is the SQUID – a highly sensitive magnetic field detector first demonstrated in the early 1970s. SQUIDs (Silver and Zimmerman, 1965) operate through a combination of superconductivity and the *Josephson effect* (Josephson, 1962, Josephson, 1974). A SQUID typically incorporates two Josephson junctions on either side of a superconducting loop, shown in Fig1a. A comprehensive review of the SQUID circuitry can be found in (Fagaly, 2006).

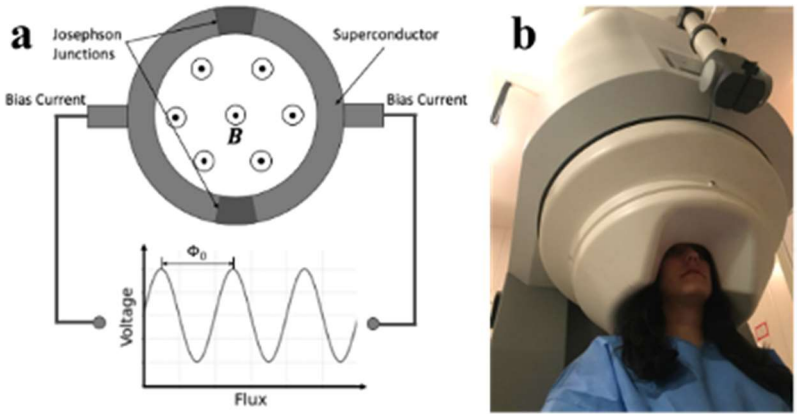

Fig. 1 The SQUID-MEG system: a) A diagram of the SQUID circuitry required to measure magnetic field, **B**, b) a CTF 275-channel SQUID-MEG system (Boto et al., 2018)

SQUIDs have ideal properties for MEG measurement: high sensitivity, with a noise floor below 10 fT/sqrt(Hz); a large bandwidth of approximately 0–12,000 Hz, covering all neural frequencies of interest; and a high dynamic range of up to 1 microtesla, meaning measurements can still be made, even in the presence of non-zero temporally stationary (DC) magnetic fields (as long as the sensors do not move). Commercially-available MEG systems comprise an array of several hundred SQUIDs housed in a helmet (e.g., Fig.1b), allowing for whole-head coverage. Typically, the SQUIDs do not measure fields from the brain directly, but they are instead inductively coupled to a superconducting flux transformer. These are usually configured either as a magnetometer or gradiometer. Magnetometers comprise a single wire wound loop placed close to the head; gradiometers comprise two loops, separated (either radially or tangentially) by some baseline distance. Reverse winding means that the measurement represents the magnetic field difference between the loops. Gradiometry reduces the influence of environmental interference and therefore increases the signal-to-noise ratio (SNR) of the MEG data. However, this comes at the cost of some depth resolution in the brain. Systems have been based on magnetometers, gradiometers, or on a mixture of the two and all have been successful in characterising the brain's magnetic field. However, whilst tried and tested, these systems are highly complex with the combination of SQUIDs, flux transformers, control electronics, and cryogenics. In addition, all MEG systems are housed within a magnetically shielded room (a room whose walls are constructed from multiple layers of high magnetic permeability (mu-metal) and high conductivity (aluminum or copper) metals). These magnetically shielded environments reduce magnetic interference impinging on the sensors, and hence maximise sensitivity to the extremely small neuromagnetic fields of interest.

SQUID-MEG has yet to reach widespread clinical uptake due to a number of limitations. Firstly, the set-up cost, which include magnetic shielding and com-

plex SQUID circuitry, make systems expensive to build. To maintain the low operational temperatures, expensive and non-renewable cryogenic cooling with liquid helium is usually required. Although this can be reduced using cryocooling systems, these new technologies are also associated with high purchase costs and are energy demanding (Lee et al., 2017). Furthermore, the sensors are fixed in position within a one-size-fits-all helmet. Results, therefore, vary due to differences in head-size; for example, children have a much greater brain-to-sensor separation than adults. Consequently, scanning those with smaller heads results in a substantially lower measured signal, and therefore SNR, due to the inverse square relationship between magnetic field and distance from the source. Custom pediatric MEG systems have been developed and built with smaller helmets; however, these are an additional expense that excludes adult-use (Okada et al., 2016). Even for a participant whose head fits the helmet perfectly in a system, there remains a required stand-off distance of ~17 mm to maintain an insulating vacuum between the cryogenically-cooled sensors and the scalp. In most individuals (who do not fit the helmet perfectly), coverage of the brain is highly inhomogeneous, with the poorer coverage typically in the frontal regions.

Finally, due to the fixed sensor positions, any head movement relative to the array can degrade data quality. To hold the head still, 3D-printed casts specific to the individual have been designed using anatomical MRIs to create the scenario where each participant fits the scanner helmet perfectly. While this does not reduce the brain-to-sensor separation, it provides additional padding to dramatically reduce movement (Troebinger et al., 2014, Meyer et al., 2017). Alternative methods for eliminating the effects of head movement, such as using post-acquisition regression algorithms, have successfully preserved data quality during small movements (Messaritaki et al., 2017). However, algorithms cannot compensate for the several-centimetre natural movements that could be made with a wearable system, where head movement is large enough to alter the SNR of the acquired data.

In sum, SQUID-MEG systems offer a very powerful and effective route to the measurement of brain function. However, limitations in current technology – specifically the requirement for cryogenic cooling of sensors – makes the current generation of systems expensive, limited in performance, and difficult to deploy, especially in certain populations.

b. Why OPMs are the stand out replacement

In recent years, several promising alternatives to SQUIDs for detecting MEG signals have been introduced. Advances in superconductivity have seen the introduction of *high-Tc SQUIDs*, which have a higher critical temperature, meaning they can operate at liquid nitrogen temperatures (77 K), rather than liquid helium temperatures (4 K). This reduces the required size of the insulating gap between the sensor and the scalp to less than 1 mm (Öisjöen et al., 2012), resulting in greater

signal magnitude. Unfortunately, high-Tc SQUIDs still require nitrogen cooling in a cumbersome dewar and are therefore still difficult to deploy as scalp-mounted, wearable systems. *Nitrogen Vacancy* (NV) magnetometers offer a promising flexible alternative. By isolating the electronic spin of an NV centre, these systems become sensitive to very weak magnetic fields, which could be exploited to measure brain activity (Rondin et al., 2014, Barry et al., 2020). NV magnetometers function at room temperature and can be miniaturised to be housed in casings that can sit on the scalp. However, at the time of writing, the sensitivity at room temperature remains lower than that of SQUIDs, achieving multiple pT/sqrt(Hz) noise floors, compared to <10 fT/sqrt(Hz) for a SQUID (Chatzidrosos et al., 2017).

In contrast, OPMs successfully achieve comparable sensitivity to conventional SQUIDs whilst maintaining an external temperature close to body temperature. Theoretically, the sensitivity could exceed that of SQUIDs to reach sub fT/sqrt(Hz) (Dang et al., 2010). Additionally, they have already been miniaturised to allow on-scalp placement (Sander et al., 2012), and commercialised (Shah and Wakai, 2013, Osborne et al., 2018, Pratt et al., 2021), with a multi-channel, whole-head OPM-based MEG system already costing less than the price of a conventional SQUID-MEG system. The bandwidth of OPMs - 0–150 Hz - while lower than that of SQUIDs, still covers the range of frequencies of interest in most MEG studies (Baillet, 2017) (though OPMs may struggle to reach the frequency of, e.g. fast ripples [~300-600 Hz] that have been measured using SQUIDs). The dynamic range of the current commercially available sensors is approximately ±1.5 nT. While this is limited (see below), additional methods of background magnetic field control allow sensors to work without exceeding this range (see below). For these reasons, OPMs have emerged as the stand out alternative to SQUIDs for use in the next generation of MEG instrumentation.

2. Technical challenges

a. What an OPM for MEG should look like

OPMs themselves are incredibly versatile, and there exist a number of different designs. Most are based on the same principle (Hanle, 1924); a gas of alkali atoms (usually Rb) is housed in a glass cell. Laser light, tuned to the D1 transition, is shone through the vapour and atoms pumped into a specific quantum state in which their magnetic moments become aligned with the beam. The gas is, therefore, “magnetic” and interacts with external magnetic fields. Specifically, in a zero-field environment, the vapour becomes completely transparent to laser light, and so the intensity

of light passing through the cell is maximised. However, if an external field impinges on the cell, atoms can escape their quantum state. Consequently, laser light is absorbed again, causing a drop in intensity passing through the cell. In this way, monitoring the passage of laser light provides a sensitive measure of magnetic field. OPMs are typically operated in the so-called Spin Exchange Relaxation Free (SERF) regime to maximise sensitivity (Shah and Romalis, 2009). The magnetic field within the cell is controlled via a set of three orthogonal electromagnetic coils which surround the cell. Most OPMs currently being used for MEG employ this basic measurement principle. However, there are many possible variations on the theme, and precisely what an OPM should "look like" for MEG measurement is still a topic of debate. Here, we outline some of the key discussion points in that debate.

i. Single-axis vs triaxial

In conventional MEG, sensors typically measure a single vector component of the neuromagnetic field, oriented (approximately) radially with respect to the head surface. This is out of necessity since it is challenging to orient bulky pick-up coils to measure the complete field vector. It is also sensible since the radial component of the neuromagnetic field has been shown to be the largest in amplitude (Iivanainen et al., 2017). This said, SQUID-MEG systems have been built that measure the full vector magnetic field at multiple locations or across the whole head (Haueisen et al., 2012, Nurminen et al., 2013). However, these triaxial sensors have not been widely adopted, potentially due to their complexity.

As OPMs do not rely on pick-up coils, sensors can be adapted to make triaxial measurements without significantly increasing their overall size. Briefly, the directional sensitivity of an OPM is provided by a known oscillating magnetic field applied along a direction orthogonal to the laser axis as it passes through the vapour. Even with a single laser beam, two independent field measurements can be made in two orientations orthogonal to the beam direction. To make triaxial measurements, the laser beam can be split to direct two perpendicular beams through the same cell, enabling (in principle) triaxial field characterisation. Sensors can also be designed with the sensitive axis dependent only on the axis of the applied modulation field, making it possible to switch the measured magnetic field vector component by simply changing the direction of the modulation (Borna et al., 2020). Consequently, unlike SQUIDs, it is simple to conceive triaxial OPMs, which measure all three components of the field at the same location in space.

Simulations have shown that measuring only the tangential axis of the MEG signal has a lower SNR than the radial component (Iivanainen et al., 2017). In addition, in most MEG studies, researchers aim to reconstruct 3D images of brain activity. This relies on accurate modelling of the magnetic fields generated by neural current (known as the forward model). Previous work has shown that it is more challenging to model tangential, compared to radial, magnetic fields (because tangential fields are more affected by "volume" current flowing in the extracellular

space and thus become more dependent on accurate modelling of conductivity). Consequently, a system measuring tangential fields is likely to be more sensitive to errors and approximations made in the forward model (Iivanainen et al., 2017). For this reason, it could be argued that OPMs for MEG need only measure the radial component of the field, ignoring the tangential components that are difficult to model.

However, measuring the tangential components alongside the radial component, whilst only providing a modest amount of extra information on fields from the brain, generates a significant amount of additional information on the non-brain (interference) sources. In short, the additional tangential components reduce the correlation of the forward fields between the source of interest in the brain and an external interfering source, and this can be exploited when reconstructing sensor space data into 3D images of current distribution in the brain. Indeed, simulations and experimental recordings have shown that a triaxial system provides a marked improvement in discrimination between signals from within the brain and external interference compared to an array of single-axis OPMs (Brookes et al., 2021). Further, in a wearable system, simulations suggest that movement artefact (fields generated as a result of the head moving with respect to some small remnant background field – see also below) might be better cancelled if triaxial sensor design is used. Further still, in cases where only a limited number of OPMs are available, triaxial sensors will improve the homogeneity of brain coverage. Therefore, with a well-characterised forward model, a triaxial sensor array (at least in theory) provides considerable advantages over a single-axis recording.

ii. Magnetometer vs. gradiometer

The majority of conventional MEG systems employ gradiometry. This may include axial gradiometers (where the magnetic field is measured at the head surface, and then some distance [usually ~ 5 cm] away); planar gradiometers (where the magnetic field is measured at two locations on the head surface) or "higher order" gradiometers where a reference array located distal to the head is used to measure background fields. In all cases, the principle is to enhance sensitivity to nearby sources of field (i.e. sources in the head) and reject common-mode interference (i.e. distal sources whose field does not vary rapidly in space). The ubiquity of gradiometers in conventional MEG, therefore, begs the question of whether gradiometers should be used in OPM-MEG.

It is conceptually simple to imagine OPM gradiometers. OPMs are small, lightweight, and it would be easy to place two OPMs to form either axial or planar gradiometers. This would necessarily allow the capture of a signal which focuses on nearby sources. However, whilst digital subtraction of signals from two independent OPMs will reduce common-mode interference, it would cause an increase in random noise, which would sum across sensors (e.g. if we assume a Gaussian noise model, the random noise would increase by a factor of the square root of two).

For this reason, “true” gradiometers (i.e. one OPM which inherently measures field gradient, rather than two separate OPMs that each measure field and a digital subtraction) would be advantageous. Such OPMs have been made recently and are suited to this kind of application (Nardelli et al., 2020).

Another problem relating to gradiometry is wearability – one of the major attractions of OPM-MEG is that OPMs can be embedded in a helmet and worn by a subject allowing them to move naturally during a MEG scan. However, employing axial gradiometers (with, for example, a 5 cm baseline as in many conventional MEG systems) would make the helmet restrictively large. Planar gradiometers are less problematic in this regard since the two measurement locations are on the head surface. However, these would likely employ short baselines, which limits depth sensitivity in the brain. It is, therefore, perhaps hard to imagine a viable wearable system that measures only field gradient.

Perhaps a better solution then is to exploit the flexibility of placement of OPMs to construct reference arrays that measure background field, which is then, by some means, subtracted from the signals from OPMs mounted on the head. This “synthetic gradiometry” approach has been shown to work (Boto et al., 2017). It will likely form a useful balance between magnetometers, which are susceptible to interference, and true gradiometry, which may be difficult to deploy in wearable systems. Alternatively, it is possible to think of ways to conceive of OPMs that simultaneously measure field and planar gradient.

iii. Nascent OPM designs

At the time of writing, a number of different types of excellent, highly sensitive OPMs have been fabricated and used successfully for MEG measurement. Single-axis sensors, such as the four-channel module shown in Fig.2c, and dual-axis sensors, like the commercial QuSpin sensors shown in Fig.2a, have been available for some years and are highly effective for MEG measurement. A triaxial sensor module design is shown in Fig.2d, where a single casing contains nine vapour cells in rows of 3, where each row is sensitive to a separate orthogonal axis (Pratt et al., 2021). As noted above, researchers have also designed optically-pumped, first-order gradiometers, with an example of this shown in Fig.2b. In this example, two vapour cells are spatially separated within the sensor to form the gradiometer, albeit with a short (2 cm) baseline (Nardelli et al., 2020).

At present, it is not clear which sensor type will be the best for MEG; conventional MEG systems would point to gradiometers as in Fig.2b, and these would be extremely effective in static systems but may be hard to deploy in wearable systems. Nascent research suggests triaxial measurement may offer advantages, particularly in terms of rejection of interference. Overall, the OPMs that are now available already offer practical ways to explore all possible combinations and permutations of array design, and this promises to be an exciting and fruitful area of research.

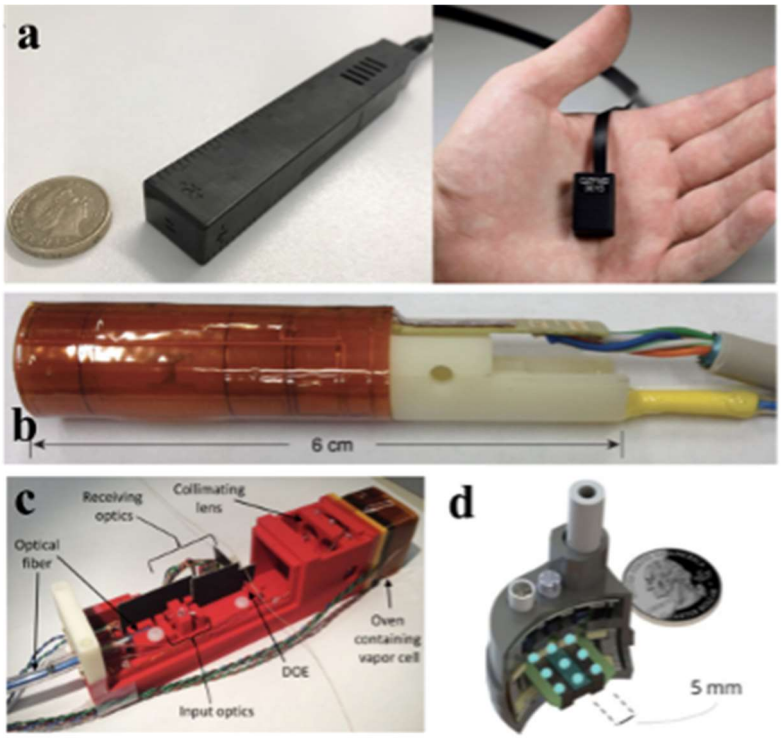

Fig. 2 OPM implementations: a) a QuSpin Gen 1 dual-axis OPM sensor (left) and Gen 2 dual-axis OPM sensor (right) (QuSpin Inc.), b) a first-order optically-pumped gradiometer (Nardelli et al., 2020), c) a four-channel OPM sensor module, where DCE refers to the diffractive optical element (Colombo et al., 2016), d) a diagram of the Kernel Flux sensor unit with a size comparison of a USD quarter dollar coin (Pratt et al., 2021)

b. Designing OPM sensor arrays for MEG

When designing an OPM-MEG system, the method with which the OPM sensors are mounted onto the head is critical. There are four key considerations to balance when optimising this design (Hill et al., 2020). 1) The helmet should hold the sensors rigidly (limiting relative movement) to avoid artefacts, and close to the scalp to maximise the measured signal. 2) Sensor locations and orientations relative to the participant's head must be known accurately to enable high fidelity modelling and, consequently, source localisation. 3) The helmet must be ergonomic and practical – particularly for subject groups such as infants or patients – this is particularly important for wearable systems. 4) As most OPMs are heated to operate in the SERF

regime, the helmet should allow heat to dissipate. This section describes the evolution of helmet designs from personalised 3D-printed scanner-casts with region-specific arrays to a generic adult helmet.

i. Region-specific OPM-MEG arrays

In early OPM demonstrations, sensors were relatively large and their cabling heavy, making whole-head wearable arrays impractical. Therefore, MEG studies were conducted using a high-density array over limited regions of interest. For example, Boto et al. used a 13-channel system to cover the right sensorimotor cortex during a left-hand index finger abduction task (Boto et al., 2018). Likewise, Iivanainen et al. (Iivanainen et al., 2020) used eight static OPMs over the back of the head to measure gamma-band effects in the visual cortex. In both cases, the sensors were intentionally placed over the region of the brain associated with the task. An example of this type of helmet design is shown in Fig.3a, and the corresponding images showing changing current density in the brain in response to a simple finger movement are shown in Fig.3b. Fig.3c shows the time course of changing oscillatory amplitude; in the time-frequency plot, red represents an increase in neural oscillatory power relative to baseline, blue represents a decrease. Line plots on the right-hand side show the difference in beta band (13-30 Hz) amplitude between a trial where the participant moved their fingers (blue) and a rest trial (red). Notice here the well-known effect whereby during movement (0-1 second time window), we see a loss in oscillatory power in the beta band, which is restored via a "rebound" (increase above baseline) post-movement.

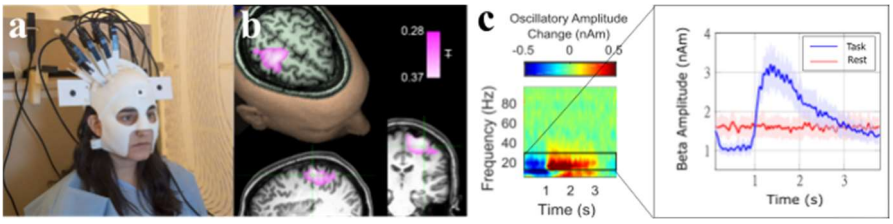

Fig. 3 Region-specific OPM-MEG: a) A photograph of the participant wearing the personal 3D-printed scanner cast with sensors over the right sensorimotor cortex, b) beamformer images showing localisation of the left finger abduction task beta response to the right motor and pre-motor cortex, c) time-frequency spectrogram (left) and line plot showing the modulation of the beta band (right) during the task period (blue) and rest (red) (Boto et al., 2018)

This design provides dense coverage over the region of interest, resulting in a high spatial resolution for source localisation in this area while working with limited sensors. This remains a valuable solution, particularly if the number of OPMs is limited or particularly high spatial resolution over one specific area is sought. However, as OPM sensors become more widely available, whole-head arrays where one

does not have to specify regions of interest *a priori* are preferable. Indeed whole-head arrays provide coverage across the entire brain, allowing, for example, the evaluation of functional connectivity, which cannot be achieved by region-specific arrays (Boto et al., 2021).

ii. Fixed or wearable arrays

Fixed helmets (i.e. where participants insert their head into a static array of OPMs) have been designed for OPM-MEG measurements (Boto et al., 2017, Borna et al., 2017, Iivanainen et al., 2020, Nardelli et al., 2020), with experimental set-up resembling SQUID-MEG. Examples are shown in Fig.4a and 4b. Such helmets can hold the sensors close to the scalp; indeed, in Fig.4b, the helmet design included moveable sensor holders, so the spatial morphology of the array can be changed to fit different head shapes. In this way, static helmet design realises many of the well-known advantages of OPMs, including higher spatial resolution, higher signal strength, and adaptation to different head shapes and sizes. In addition, a static array is more straightforward because it does not move relative to a background field (which generates magnetic artefacts – see below). However, a fixed array means participants must remain still for long periods (similar to SQUID-MEG and fMRI), and so this removes a major OPM advantage. Wearable arrays are more complex to fabricate since one must give significant thought to helmet weight and cable management, and the background field must be controlled. However, wearable arrays provide access to patient groups who find it hard to remain still and also enable the introduction of novel paradigms. It is, of course, possible to conceive of a system that offers both static and wearable arrays using the same OPMs – thus providing the best of both worlds.

iii. 3D-printed individual scanner-casts

Some of the early wearable OPM-MEG arrays used 3D-printed scanner-casts, unique to each participant. To design these, an anatomical MRI of the participant's scalp is used to create a “made-to-measure” helmet, fitting the participant's head and face perfectly. This close fit reduces movement between the head and the helmet to a minimum, holding sensors fixed in a rigid position relative to the brain. Sensor holders are incorporated into the helmet shape, either over regions of interest as in Fig.3a or across the entire scalp, as in Fig.4c. The fact that the 3D-printed scanner-cast is based on the MRI, and is represented digitally, means that the sensor locations relative to the brain are known to a high degree of accuracy; thus, co-registration (see box) is not required.

Co-registration

Co-registration is the method by which the location and orientation of the OPMs are determined in reference to the participant's brain. This allows magnetic field patterns measured by the sensors to be transformed into the reference frame of a structural MRI, and field modelling allows for localisation of the underlying neural current. An accurate co-registration, where the sensor positions/orientations are known with millimetre/degree precision, is critical. In individualised scanner-casts this information is known a priori. However, when using generic helmets, a more complex surface matching procedure is typically needed where the location of the head within the helmet is found either via a 3D optical scan or via digitisation.

Individualised scanner-casts provide the perfect solution: they are comfortable to wear, relatively lightweight, hold sensors in the ideal position close to the scalp, and are rigid; therefore, OPMs cannot move relative to one another during a scan. However, each cast's design process can be expensive and time-consuming, and 3D-printing fees can be high. In addition, they can take time to produce (one cannot perform the anatomical MRI and the MEG recording on the same day). As the scanner-casts are designed using a single participant's MRI, only a single person will fit each helmet, making their use in large scale studies (with many participants) wasteful and potentially impractical due to the high cost. Despite this, individualised scanner-casts are in use in pioneering clinical studies (Vivekananda et al., 2020).

iv. Generic caps and helmets

To reduce the costs and production time for 3D-printing individualised helmets, generic helmets designed to fit multiple participants have been developed. An early example of this involved adapting adult bicycle helmets to hold sensors (Hill et al., 2019). Each bicycle helmet cost only a fraction of the cost of a 3D-printed scanner-cast and fitted multiple participants with different head shapes. In addition, children's bicycle helmets were adapted, as shown in Fig.4d, and used with a region-specific array to demonstrate lifespan compliance (i.e., the ability for this technology to be used with people across all ages) of OPM-MEG. However, the foam padding in the bicycle helmet (designed to protect the head from impact) was thermally insulating and consequently prevented the dissipation of heat from the sensors. Thus, during longer scans, heating became an issue. In addition, the helmets were not designed to hold sensors; therefore, structural integrity was impaired when slots were added across the whole head. Further, the helmets did not come far enough down the sides of the head to capture fields from, e.g. some temporal or occipital regions. So, whilst the bike helmet idea is cheap and practical, complete head coverage is problematic.

An "EEG-style" flexible cap, mounting up to 63 sensors, was manufactured by QuSpin Inc (Colorado, USA) and is shown in Fig.4e. The elasticated fabric enables stretching of the cap to adapt to different adult head sizes. Plastic boning is

sewn into the material to maintain shape and rigidity and to reduce OPM movement relative to the scalp. Sensor mounts hold the sensors at their corners, so heat can readily escape through convection from the sensor surfaces. The cap is very lightweight and ergonomic, with a total weight of 309 g when containing 49 QuSpin Gen-2 OPM sensors. However, the flexibility means that sensors could move relative to one another, which generates artefacts that are hard to remove. Further, the flexible nature complicates the co-registration process since, rather than finding the spatial relationship between the head and a single solid helmet, we must find the location of every OPM separately. This gives rise to a co-registration error that is random across sensors – these errors have been shown to be problematic for source localisation (Hill et al., 2020). An additional limitation is a requirement to remove and replace all sensors between experiments for co-registration, which requires a substantial amount of time.

Additively-manufactured rigid generic helmets have also recently been trialed. In the example shown in Fig.4f, the inner surface was designed from a set of adult MRIs to accommodate most adult heads. Removable padding and a chin strap reduce helmet motion relative to the head. The helmet provides 133 possible sensor holders, which rigidly hold an OPM at its corners, preventing any sensor movement with respect to all other sensors but also allowing heat dissipation. Crucially, the fixed sensor holders provide a highly accurate measurement of the relative locations and orientations of the sensors. This simplifies the co-registration procedure. Between sensor holders, a lattice design with a lightweight material facilitates heat convection and reduces the pressure on the head, neck and shoulders during scanning by limiting weight. So far, this generic solution proved a useful means to adapt OPM-MEG to large cohort studies; it is possible to envisage a situation where similar helmets are made in multiple sizes (Hill et al., 2020). However, solutions that allow some degree of sensor travel in the radial direction potentially offer a better final solution.

Fig. 4 The evolution of the helmet design: Photographs of a) a static, 3D-printed helmet (Iivanainen et al., 2020), b) a fixed 3D-printed helmet with moveable sensor holders to conform to different head shapes (Nardelli et al., 2020), c) a whole-head 3D-printed personal scanner-cast (Barry et al., 2019), d) a children bike helmet (Hill et al., 2019), which has been modified to hold OPM sensors, e) a flexible, EEG-like cap (Hill et al., 2020), and f) a generic 3D-printed helmet based upon averaged adult MRI scans (Hill et al., 2020)

Co-registration

As noted above, generic helmets require a co-registration procedure. Whilst an additional source of error, such procedures are commonplace in conventional MEG and indeed some EEG studies. The standard SQUID-MEG co-registration uses a combination of head position indicator (HPI) coils attached to the participant's head during the scan and a pen-like 3D digitiser. The HPI coils are localised with respect to the MEG sensors by driving known currents through the coils during the MEG acquisition. The coil locations relative to the (fixed) MEG sensors are then found using a magnetic dipole fit. Following the scan, the position of the HPI coils and a set of anatomical landmarks are digitised. The final co-registration aligns the HPI coil locations from the MEG acquisition with the position of the anatomical landmarks on the corresponding MRI scan, resulting in complete co-registration of MEG sensor locations to brain anatomy.

There is no reason why the above procedure cannot be used for OPM-MEG. However, to date, most OPM co-registrations have followed the optical imaging technique first pioneered by Zetter et al. (Zetter et al., 2019). Briefly, a 3D optical imaging system (such as the structure IO camera [Occipital Inc., San Francisco, CA, USA] with an Apple iPad and Skanect software) is used as a time-efficient and accurate way to generate a 3D representation of the head/face surface. The structured-light scanner projects an infrared light pattern onto an object; reflected light is then detected by a camera. The 3D shape can be determined by the distortion of the reflected pattern. Markers are placed at known locations on the helmet and the participants face. First, a 3D digitisation is taken with the participant wearing the helmet, and the location of the helmet relative to the markers on the face is determined. Following this, the helmet is removed, and a second scan is acquired. This provides the location of the coloured markers on the face relative to the head surface. The head surface from this digitisation is fitted to the anatomical MRI scan. Along with the helmet-to-face mapping, this then provides the complete transformation required to map the helmet to the MRI. As the locations and orientations of sensors in the helmet are known *a priori*, this offers a full co-registration of the sensors to the brain anatomy (Hill et al., 2020).

v. Crosstalk

Crosstalk, in the context of OPM-MEG, is an effect whereby the magnetic field measured by one OPM is altered by the presence of a second OPM. This is a significant consideration when designing arrays containing large numbers of sensors. OPMs contain on-board electromagnetic coils which can control the magnetic field within the vapour cell. Both DC and AC magnetic fields are generated: the DC fields null the ambient magnetic field to maintain the SERF regime. The AC (modulation)

fields are required to give an OPM its directional sensitivity. It is essential that modulation fields align precisely with the required sensitive axis of the OPM. However, the fields generated by Helmholtz coils not only affect the vapour cell but also spread outside the sensor casing and will impinge on other OPMs in close proximity. Modulation fields across all OPMs in an array tend to be coherent, meaning they interfere constructively; thus, if two OPMs are operated in close proximity, modulation fields can become distorted and consequently, either sensor gain, or sensitive axis orientation can be affected. In practice, calibration procedures can help ameliorate this effect. In addition, with current OPM arrays, sensor separations have been sufficient that crosstalk has been relatively well controlled. However, as OPM arrays become more densely packed, or as researchers begin to employ OPM-MEG in infant populations (where smaller head sizes will likely mean denser sensor packing), this problem is likely to become more significant.

c. Suppressing background magnetic fields

One drawback of OPMs for MEG measurement is their relatively low dynamic range; specifically, most OPMs cannot cope with field changes above ~1.5 nT (Boto et al., 2018). Consequently, a low magnetic field environment is required. This is especially crucial in wearable systems where OPMs are expected to move, as translation through a residual magnetic field of just a few nT can saturate sensor outputs. In a typical unshielded environment, the Earth's magnetic field is ~50 μT, and temporally varying magnetic fields are produced by, e.g. electronic equipment, which is orders of magnitude larger than fields from brain activity. This section describes methods for reducing both the static and dynamic background magnetic fields to enable wearable OPM-MEG.

i. Magnetically-shielded environments

Magnetically-shielded rooms (MSRs) are used to shield both SQUID and OPM-MEG systems from magnetic interference, improving the SNR. MSRs employ multiple layers of materials chosen for their specific properties to shield from static (DC) and temporally varying (AC) magnetic fields. With this method, shielding materials are used to change the structure of the magnetic field from interfering sources, diverting lines of magnetic flux away from the area where a low magnetic field is intended (Hoburg, 1995). Shields are characterised by the shielding factor,

$$SF = \frac{|B_0|}{|B_S|}, \tag{2.1}$$

where B_0 is the unshielded field, and B_S is the shielded field. A larger shielding factor corresponds to better shielding. Two physical mechanisms, requiring two different material properties and shielding factors, are used in MSRs.

DC fields

For low-frequency or DC fields, a material with a high magnetic permeability, μ_r, is used to divert flux away from the shielded region, using a mechanism known as flux shunting. This effect arises due to the boundary between materials of different relative magnetic permeability. Ampere's law dictates that the tangential component of the magnetic field **H** must be continuous across the surface of the material, and Gauss's law states that the normal component of **B** must also be continuous. Inside the material, **B** takes the form $\mathbf{B} = \mu_0\mu_r\mathbf{H}$, whereas $\mathbf{B}\sim\mu_0\mathbf{H}$ in the air. For high permeability materials, the magnetic field rapidly changes direction at the interface between the materials to satisfy the boundary conditions. This results in magnetic flux lines being 'pulled in' perpendicular to the material and then 'shunted' along the material surface before being released back into air. The shielding factor for a shield of such material is dependent on its magnetic permeability, the dimensions of the shield and the area enclosed by the shield. For example, for a spherical shield with inner radius a and outer radius b, the shielding factor across the shielded volume will be (Hoburg, 1995)

$$SF = \frac{(\mu_r + 2)(2\mu_r + 1) - 2\frac{a^3}{b^3}(\mu_r - 1)^2}{9\mu_r}. \tag{2.2}$$

For material with high magnetic permeability, equation 2.2 can be simplified when the thickness of the shield, $\Delta = b - a$, is small compared to the inner radius and $\mu_r\frac{\Delta}{a} \gg 1$ to

$$SF \approx \frac{2}{3}\mu_r\frac{\Delta}{a} + 1\,, \tag{2.3}$$

(Cohen, 1970). This approximation reveals a decrease in the DC shielding factor for larger shield sizes if the thickness remains constant. Multiple layers of high-permeability materials can be used with spaces between the layers to improve the shielding factor by an order of magnitude or more.

AC fields

A material with high electrical conductivity (copper, for example) is used to shield the higher frequency ($\sim >$10 Hz) AC fields via eddy current cancellation. The time-varying magnetic flux density, **B**, induces an electric field, **E**, within the material due to Faraday's Law,

$$\nabla \times \mathbf{E} = -\left(\frac{\partial \mathbf{B}}{\partial t}\right). \quad (2.4)$$

For materials with high electrical conductivity, σ, this electric field induces a current density within the material, which induces magnetic flux that opposes the change in the imposed magnetic flux. The imposed and induced magnetic flux superimpose and cancel, expelling the total flux out of the conducting material and the intended shielded region. For an AC field with angular frequency $\omega = 2\pi f$, the induced current density and total flux density decay exponentially into the material and shielded region with a characteristic decay length, or "skin depth"

$$\delta = \sqrt{\frac{2}{\omega \mu_0 \mu_r \sigma}}, \quad (2.5)$$

where μ_r is the relative magnetic permeability of the material. For time-varying magnetic fields, the shielding factor is complex, showing a frequency dependent phase variation, and can be expressed as

$$SF = 1 + i\omega \frac{\mu_0 \sigma a \Delta}{3}, \quad (2.6)$$

for a spherical enclosure, when $\mu_r = 1$, $\delta >> \Delta$ and $\Delta << a$. The shielding improvement here contrasts with the flux shunting case, since the AC shielding factor increases with radius for a fixed shield thickness.

Degaussing

The high permeability materials used in the MSR (e.g., mu-metal) are often alloys of metals such as iron or nickel, making them ferromagnetic. When the MSR is exposed to magnetic fields, this can leave a remnant magnetisation in the shielded region. To reduce this remnant magnetisation, a process of degaussing is employed (Kelly, 1946). Large coils are wrapped around the room, through which a decaying oscillatory current is applied. This drives the ferromagnetic metal around hysteresis loops of diminishing area, suppressing the remnant magnetic field and improving the performance of the magnetic shielding.

Towards smaller shielded enclosures

The methods above are highly effective in reducing both DC and AC fields. Almost all conventional MEG systems exist with rooms of this type (usually comprising two layers of mu-metal and one of conductive material (e.g. Cu or Al). These MSRs reduce DC fields to ~30 nT (without degaussing) or ~2 nT with degaussing); AC fields are reduced to a level <10 fT/sqrt(Hz) at frequencies above a few Hz. Such enclosures provide the perfect space for (conventional) MEG acquisition. However, SQUID-MEG systems are large and cumbersome, and this, coupled with the need for access for liquid helium fills, makes MSRs large and expensive. Without the

need for a sizeable cryogenic dewar, OPM systems can be shielded using much smaller, lighter and cheaper, magnetic shielding. Human-sized, cylindrical magnetic shields (Fig.4b) have been constructed for OPM-MEG experiments, with an open-end for access. Following the same design as the MSR, layers of DC and AC shielding materials are fashioned into a cylindrical shape rather than a larger room. This reduces the space requirement and, crucially, lowers the cost. The cylindrical shields can house additional electromagnetic field nulling coils built into the shield to provide further ambient magnetic field control (Borna et al., 2017). Similarly, smaller MSRs have also been proposed (cercamagnetics.com), with a footprint of ~1.5 m x 1.5 m. These smaller rooms are much less expensive than conventional MSRs, whilst also offering excellent performance. These nascent shielding options point the route to cheaper and more widely deployable MEG devices.

ii. Using coils to null the static remnant magnetic field

While MSRs are efficient in reducing magnetic field, the residual field inside many MSRs remains too high for OPM operation in a wearable system. Specifically, without degaussing, even in a highly efficient shielded room (SF ~ 2,000), the background field would be of order 25 nT, and consequently, just a 4 degree rotation of an OPM would cause a field shift large enough to take the OPM outside its dynamic range. With degaussing (SF ~ 20,000), background fields are closer to 2 nT. However, even in this ultra-low field environment, magnetic artefacts from small movements will be larger than brain activity, and a 90 degree head rotation would take an OPM outside its dynamic range. For these reasons, to achieve the required background magnetic field, further shielding (beyond what can be achieved with passive techniques) is required. Recent OPM developments have employed field nulling techniques based on the use of electromagnetic coils, e.g. Fig.5 (Holmes et al., 2018, Iivanainen et al., 2019, Borna et al., 2020).

The basic scheme is to measure the residual field inside a magnetically shielded enclosure and then use coils to generate a field equal and opposite to that measured, thus cancelling it out. However, a challenge in coil design is to find a way to generate magnetic fields in all three Cartesian orientations. Conventionally this would be done with a Helmholtz-like set-up. Indeed this proves effective (Iivanainen et al., 2019) (Fig.5a). However, it means enclosing the participant since coils must be mounted on six planes surrounding the subjects. An elegant solution to this is a bi-planar coil system (Fig.5b) which provides a more open scanning environment. Here, the coil design is based upon a harmonic minimisation method (Carlson et al., 1992), which has been used previously in MRI. This approach was adapted to compensate all three Cartesian components of the uniform background field and the spatial gradients in the MSR whilst restricting coils to two planes placed on either side of the subject.

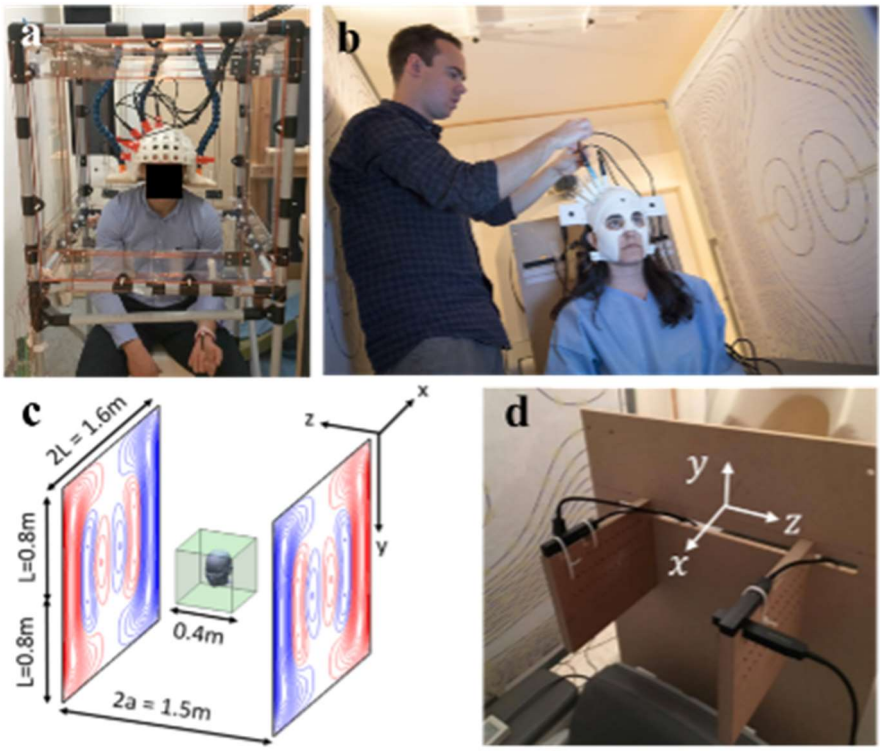

Fig. 5 The active nulling coil system: a) a photograph of a Helmholtz cage coil design (Iivanainen et al., 2019), b) a photograph displaying a participant within the bi-planar coil system (Boto et al., 2018), c) a diagram of the bi-planar coils; the green box shows the nulled region and the geometry of the two coils are provided, with the wire paths for the coil compensating for the static field in the 'x' orientation shown on the faces (Holmes et al., 2018), d) the OPM reference array (Holmes et al., 2018)

From Maxwell's equations for magnetostatics, in a current-free region the magnetic field obeys

$$\nabla . \mathbf{B} = 0, \tag{2.7}$$

and

$$\nabla \times \mathbf{H} = \mathbf{J}, \tag{2.8}$$

where $\mathbf{J}$ is a current density. In the air enclosed by the shield, $\mathbf{B} = \mu_0 \mathbf{H}$ and no current density exists, consequently

$$\nabla \times \mathbf{B} = 0. \tag{2.9}$$

Evaluating these equations, the magnetic field can therefore be expressed as three vector components, B_x, B_y, B_z. These each obey Laplace's equation, so they can be represented as a series of spherical harmonics, with the lowest order terms corresponding to spatially uniform magnetic fields and magnetic field gradients.

Due to a high degree of symmetry between the lowest order terms, a series of just eight components are required to fully describe the uniform magnetic fields

and linear magnetic field gradients, rather than the expected twelve (Holmes et al., 2018). Therefore, three coils can be designed to produce the three uniform field vector components and a further five coils designed to generate the field gradients. Each coil produces a homogenous magnetic field or field gradient (to within 5%) inside a 40-cm length cube, highlighted by the green region in Fig.5c.

In Holmes et al. 2018, a reference array with four OPMs was set up around the participant to measure the remnant magnetic field inside the MSR, as shown in Fig.5b and d. Using the two sensitive axes, the four OPMs can measure the three vector field components at two separate spatial locations, 30 cm apart. From this, a linear combination of the vector components and field gradients that best model the measured field can be determined. Feedback controllers modulate the currents in the electromagnetic coils, applying an equal and opposite magnetic field based on a known value of the coil field per unit applied current. This cancels the remnant magnetic field. More specifically, the measured field and field gradients are passed to proportional integral derivative (PID) control loops for more precise control. Therefore, the current applied depends not only on the latest measurement but also on the history of the system. A desired "setpoint" value is required, which, for magnetic field nulling, is a measured magnetic field close to zero (in practice reaching around tens of pT and pT/m). The error is computed as the difference between the setpoint and the measurement. The current applied to the coils is then given as the sum of three terms. The first is proportional to the error, the second varies with the integral of the error over time, and the third with the derivative of the error. Once the residual field has been nulled, the PIDs are switched off, and a stable current is applied to the coils to maintain the nulled region. Using this method, remnant fields inside the MSR have been reduced to as low as 250 pT across a region of space in which the head is contained. These extremely low fields have been shown to enable free movement during scanning.

iii. Nulling dynamic magnetic fields

In hostile magnetic environments, such as a city-centre site, the magnetic field within an MSR also varies temporally in an unpredictable manner; (e.g. at a site in central London, this was found to be caused by passing underground trains). This causes OPMs to move outside their dynamic range, sometimes just seconds or minutes after nulling, making even short OPM-MEG scans unfeasible (Holmes et al., 2019). To counter this, a dynamic nulling system can be employed to account for the low-frequency time-varying fields or drifts (Iivanainen et al., 2019). For example, a high-speed dynamic PID controller can be used to regulate currents in the coils in accordance with measured field variation. This maintains a low ambient magnetic field within the dynamic range of the sensors. Such dynamic nulling methods will be critical if OPM-MEG is to be effectively employed at sites where magnetic environments are variable over time.

3. Applications

At the time of writing, OPM-MEG remains a nascent technology, and relatively little work has been done to exploit its advantages. Nevertheless, a small number of studies have emerged which are beginning to show that this new technology could ultimately replace SQUIDs as the fundamental building block of MEG instrumentation. Here, we review a subset of these studies briefly.

a. Novel paradigms

The motor response to ballistic movements, such as a single finger abduction, is well documented with SQUID-MEG and functional magnetic resonance imaging. However, larger whole-body movements during more natural tasks are yet to be widely studied due to the restrictive environments imposed by traditional scanners. A wearable OPM-MEG system enables brain function to be examined during more natural movements. For example, Boto et al. demonstrated this with a ball-game paradigm, during which a participant bounced a ball on a bat for 10 s, while they performed relatively large and unpredictable head, shoulder, arm and hand movements. Head motion was measured using a motion-tracking camera. Using only static magnetic field nulling with the bi-planar coils and regression using the reference array post-acquisition, beta modulation was localised to the arm and wrist area of the sensorimotor cortex during the game, despite head movements of up to 6 cm (Boto et al., 2018). This simple task could be extended to examine the neural correlates of motor coordination.

Collecting functional neuroimaging data during a combination of a virtual reality (VR) stimulation and natural movement potentially offers a transformative change for neuroscientific study. VR provides sensory input to a user, inducing a feeling of presence within a simulated environment. This is attractive for neuroscientists as the participant can be placed in almost any virtual environment imaginable, which can then be controlled, allowing for data averaging and manipulation. This, therefore, offers the prospect of new types of stimulation; for example, investigation of how the brain manages increased stress levels; or how we might navigate a virtual environment. VR is achieved by projecting two independent, spatially shifted images to the user's eyes using either a head-mounted display (HMD) or computer automated virtual environment (CAVE). These two images mimic the parallax of the human eyes and consequently make the resulting image look three dimensional. Simultaneous tracking of the position and orientation of the user's head and updating the projected images in real-time allows visual exploration of the environment. This combination of movement induced image refresh and 3D projection enables the feeling of 'presence' in VR.

Previously, VR has been successfully used to elicit brain activity measured by EEG (Tromp et al., 2018); however, EEG suffers from poor spatial resolution and data are contaminated by movement artefacts in frequency bands above 20 Hz (Boto et al., 2019). Wearable OPM-MEG offers an improvement in spatial resolution, while being approximately ten times less susceptible to interference from muscles, motivating the development of VR-MEG (Roberts et al., 2019a). However, OPMs are susceptible to interference generated by the VR head-mounted display (HMD). This is particularly problematic because, as the display depends on subject movement, it is entirely unpredictable, producing interference that is difficult to cancel. Nevertheless, Roberts et al. showed that MEG data could be recorded in the presence of such interference. A prototype OPM-MEG system employed 12 OPMs over the visual cortex and a VR HMD held over the eyes (Fig.6a). The background static magnetic field in the MSR was controlled using a bi-planar coil system, enabling free head movement in the region surrounding the head. Head movement was passively measured using a tracking camera and infrared reflectors attached to the HMD and was fed back to update the visual scene. In the virtual environment, the participant was placed behind a wall, which they could look around by leaning to the right or left to see a visual stimulus (Fig.6b). This motion meant that the stimulus itself appeared in either the left or right visual field, and in accord with the retinotopic organisation of the visual cortex, the neural response would be expected in the right or left hemisphere, respectively. Results were as expected, with functional images showing modulation in opposing hemispheres depending on which way the subject leaned. This provides proof-of-concept that a wearable OPM-MEG system can be coupled with VR.

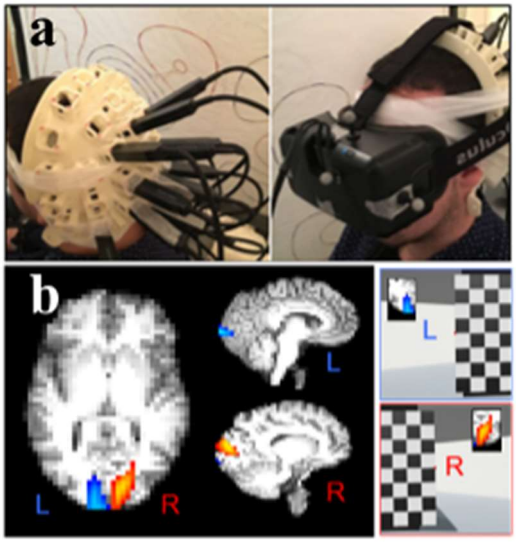

Fig. 6 OPM-MEG in a virtual reality environment: a) the OPM sensors placed on the back of the head with the Oculus Rift VR headset on the front, b) source localisation, leaning to the left, with the checkerboard presented to the right, generated left hemisphere activation (blue overlay)

and leaning right, with a left presented checkerboard, generated right hemisphere activation (red overlay) (Roberts et al., 2019a)

b. New subject cohorts

A wearable MEG system enables a more comprehensive range of participant groups to be scanned. One group of particular interest are children. The first few years of life see the development of many critical aspects of human behaviour, including movement, language, social interaction and executive function. By the end of the first decade, cognitive and attentional mechanisms and finer motor skills have evolved. Yet relatively little is known about the maturational trajectory of brain function during these critical years. The unnatural scanning environments imposed by traditional neuroimaging techniques can cause anxiety in healthy children, who struggle to remain still throughout the scanning session and become uncooperative. This effect is exacerbated when studying childhood developmental disorders, for example, autism or attention deficit hyperactivity disorder (ADHD). OPM-MEG combines a wearable system with a more natural, open scanning environment, suitable for scanning participants of all ages. Hill et al. demonstrated this with a prototype system using a small OPM array to scan children (Hill et al., 2019). The wearable OPM helmets were less intimidating than traditional scanners. The open scanning environment meant that a parent could be sat in the room with the child during the scan. However, to design a whole-head, dense OPM-MEG array for children, the crosstalk from proximal sensors, as well as aspects of head coverage such as spatial aliasing effects caused by the proximity of the brain to sensors, needs to be accounted for. This remains a topic of research.

Movement artefacts have also impacted the study of disorders that cause unpredictable involuntary movements, such as Parkinson's disease or Tourette's syndrome. Using traditional neuroimaging methods to study such conditions typically results in large amounts of data loss due to motion. With effective background field suppression to allow for movement, a wearable OPM-MEG system enables data acquisition even during the extensive and sporadic movements associated with tics or body tremors. Not only will this provide a better understanding of neurodevelopmental and neurodegenerative conditions, but it could also be instrumental in researching effective therapies.

c. Creative sensor placement

Finally, a flexible OPM array affords creativity in sensor placement, which is also beginning to be exploited. For example, Lin et al. used a specially crafted OPM array to specifically target activity in the cerebellum – something that is not widely

studied in MEG due to inadequate coverage of conventional systems in those areas (Lin et al., 2019). Further, a recent study explored the human hippocampus by holding a sensor to the roof of the mouth while simultaneously measuring magnetic fields on the scalp (Tierney et al., 2021). In simulations, hippocampal sources were found to give rise to dipolar field patterns with a minimum or maximum at the roof of the mouth. By utilising the versatility of the OPM sensors, data were acquired with a mouth sensor, which showed the greatest task-related theta power change in comparison to the scalp-mounted sensor array. These early examples show how the flexibility of an OPM array might be exploited. It should also be noted that magnetic fields are generated from many other regions of the body, including, e.g. the muscles and the spine. It is conceivable that future generations of OPM-MEG may also place OPM sensors over these other areas of the body, for example, to explore how the brain controls the body via cortico-muscular coherence.

4. Conclusion and future outlook

Functional neuroimaging is an extremely powerful means to interrogate neural activity and its breakdown in disease. However, the current toolkit is limited, either by cryogenic cooling, which makes for rigid and cumbersome systems like SQUID-MEG and fMRI, or by low spatial resolution and susceptibility to motion artefacts like EEG or fNIRS.

Lightweight and flexible OPM sensors have driven the development of wearable OPM-MEG that combines the advantages of conventional MEG with the flexibility of EEG. By operating close to body temperature, OPMs can be placed directly on the scalp surface, getting closer to the brain, therefore yielding a higher SNR and better spatial resolution than conventional MEG (which itself outperforms EEG). Moreover, the small and lightweight nature of OPMs allows for the fabrication of sensor arrays that can fit anyone. In addition, the use of electromagnetic coils and advanced shielding means that OPM-MEG systems can move with the head. The result is a measure of brain function acquired within a more natural environment opening up new opportunities to study different patient cohorts or the introduction of novel experimental paradigms.

OPM-MEG certainly has the potential to replace SQUID-MEG as a research and clinical tool. Moreover, it is more effective, more flexible, and cheaper than conventional systems meaning that its uptake could ultimately be greater; indeed, there is even potential for it to replace EEG in some applications. One good example is the localisation of interictal spikes in epilepsy. In pre-surgical planning, the localisation of the epileptic activity requires high spatiotemporal accuracy. OPM-MEG has already been demonstrated in this application, and work is underway to develop systems to look at children (Vivekananda et al., 2020). This potentially opens up avenues of immediate clinical application. Outside epilepsy, conventional MEG is already showing great promise in many areas, including mild

traumatic brain injury (Huang et al., 2014), Autism (Roberts et al., 2019b) and Schizophrenia (Gascoyne et al., 2021). The utility of MEG as a research tool is already well established. For these reasons, the future of OPM-MEG is bright, and it is hoped that it could become a mainstay technology for future investigation of the human brain and the many disorders that affect it.

References

BAILLET, S. 2017. Magnetoencephalography for brain electrophysiology and imaging. *Nature neuroscience,* 20**,** 327-339.

BARRY, D. N., TIERNEY, T. M., HOLMES, N., BOTO, E., ROBERTS, G., LEGGETT, J., BOWTELL, R., BROOKES, M. J., BARNES, G. R. & MAGUIRE, E. A. 2019. Imaging the human hippocampus with optically-pumped magnetoencephalography. *NeuroImage,* 203**,** 116192.

BARRY, J. F., SCHLOSS, J. M., BAUCH, E., TURNER, M. J., HART, C. A., PHAM, L. M. & WALSWORTH, R. L. 2020. Sensitivity optimization for NV-diamond magnetometry. *Reviews of Modern Physics,* 92**,** 015004.

BERGER, H. 1929. Über das elektroenkephalogramm des menschen. *Archiv für psychiatrie und nervenkrankheiten,* 87**,** 527-570.

BORNA, A., CARTER, T. R., COLOMBO, A. P., JAU, Y.-Y., MCKAY, J., WEISEND, M., TAULU, S., STEPHEN, J. M. & SCHWINDT, P. D. 2020. Non-invasive functional-brain-imaging with an OPM-based magnetoencephalography system. *Plos one,* 15**,** e0227684.

BORNA, A., CARTER, T. R., GOLDBERG, J. D., COLOMBO, A. P., JAU, Y.-Y., BERRY, C., MCKAY, J., STEPHEN, J., WEISEND, M. & SCHWINDT, P. D. 2017. A 20-channel magnetoencephalography system based on optically pumped magnetometers. *Physics in Medicine & Biology,* 62**,** 8909.

BOTO, E., HILL, R. M., REA, M., HOLMES, N., SEEDAT, Z. A., LEGGETT, J., SHAH, V., OSBORNE, J., BOWTELL, R. & BROOKES, M. J. 2021. Measuring functional connectivity with wearable MEG. *NeuroImage,* 230**,** 117815.

BOTO, E., HOLMES, N., LEGGETT, J., ROBERTS, G., SHAH, V., MEYER, S. S., MUNOZ, L. D., MULLINGER, K. J., TIERNEY, T. M., BESTMANN, S., BARNES, G. R., BOWTELL, R. & BROOKES, M. J. 2018. Moving magnetoencephalography towards real-world applications with a wearable system. *Nature,* 555**,** 657-661.

BOTO, E., MEYER, S. S., SHAH, V., ALEM, O., KNAPPE, S., KRUGER, P., FROMHOLD, T. M., LIM, M., GLOVER, P. M. & MORRIS, P. G. 2017. A new generation of magnetoencephalography: Room temperature measurements using optically-pumped magnetometers. *NeuroImage,* 149**,** 404-414.

BOTO, E., SEEDAT, Z. A., HOLMES, N., LEGGETT, J., HILL, R. M., ROBERTS, G., SHAH, V., FROMHOLD, T. M., MULLINGER, K. J. & TIERNEY, T. M. 2019. Wearable neuroimaging: combining and contrasting magnetoencephalography and electroencephalography. *NeuroImage,* 201**,** 116099.

BROOKES, M. J., BOTO, E., REA, M., SHAH, V., OSBORNE, J., HOLMES, N., HILL, R. M., LEGGETT, J., RHODES, N. & BOWTELL, R. 2021. Theoretical advantages of a triaxial optically pumped magnetometer magnetoencephalography system. *NeuroImage***,** 118025.

CARLSON, J., DERBY, K., HAWRYSZKO, K. & WEIDEMAN, M. 1992. Design and evaluation of shielded gradient coils. *Magnetic resonance in medicine,* 26**,** 191-206.

CHATZIDROSOS, G., WICKENBROCK, A., BOUGAS, L., LEEFER, N., WU, T., JENSEN, K., DUMEIGE, Y. & BUDKER, D. 2017. Miniature Cavity-Enhanced Diamond Magnetometer. *Physical Review Applied,* 8**,** 044019.

COHEN, D. 1968. Magnetoencephalography: evidence of magnetic fields produced by alpha-rhythm currents. *Science,* 161**,** 784-786.

COHEN, D. 1970. Large-volume conventional magnetic shields. *Revue de Physique Appliquee,* 5**,** 53-58.

COLOMBO, A. P., CARTER, T. R., BORNA, A., JAU, Y.-Y., JOHNSON, C. N., DAGEL, A. L. & SCHWINDT, P. D. 2016. Four-channel optically pumped atomic magnetometer for magnetoencephalography. *Optics express,* 24**,** 15403-15416.

DANG, H. B., MALOOF, A. C. & ROMALIS, M. V. 2010. Ultrahigh sensitivity magnetic field and magnetization measurements with an atomic magnetometer. *Applied Physics Letters,* 97**,** 151110.

FAGALY, R. 2006. Superconducting quantum interference device instruments and applications. *Review of scientific instruments,* 77**,** 101101.

GASCOYNE, L. E., BROOKES, M. J., RATHNAIAH, M., KATSHU, M. Z. U. H., KOELEWIJN, L., WILLIAMS, G., KUMAR, J., WALTERS, J. T., SEEDAT, Z. A. & PALANIYAPPAN, L. 2021. Motor-related oscillatory activity in schizophrenia according to phase of illness and clinical symptom severity. *NeuroImage: Clinical,* 29**,** 102524.

HANLE, W. 1924. Über magnetische beeinflussung der polarisation der resonanzfluoreszenz. *Zeitschrift für Physik,* 30**,** 93-105.

HAUEISEN, J., FLEISSIG, K., STROHMEIER, D., ELSARNAGAWY, T., HUONKER, R., LIEHR, M. & WITTE, O. 2012. Reconstruction of quasi-radial dipolar activity using three-component magnetic field measurements. *Clinical neurophysiology,* 123**,** 1581-1585.

HILL, R. M., BOTO, E., HOLMES, N., HARTLEY, C., SEEDAT, Z. A., LEGGETT, J., ROBERTS, G., SHAH, V., TIERNEY, T. M., WOOLRICH, M. W., STAGG, C. J., BARNES, G. R., BOWTELL, R., SLATER, R. & BROOKES, M. J. 2019. A tool for functional brain imaging with lifespan compliance. *Nature Communications,* 10**,** 4785.

HILL, R. M., BOTO, E., REA, M., HOLMES, N., LEGGETT, J., COLES, L. A., PAPASTAVROU, M., EVERTON, S. K., HUNT, B. A. & SIMS, D. 2020. Multi-channel whole-head OPM-MEG: Helmet design and a comparison with a conventional system. *NeuroImage,* 219**,** 116995.

HOBURG, J. 1995. Principles of quasistatic magnetic shielding with cylindrical and spherical shields. *IEEE Transactions on electromagnetic compatibility,* 37**,** 574-579.

HOLMES, N., LEGGETT, J., BOTO, E., ROBERTS, G., HILL, R. M., TIERNEY, T. M., SHAH, V., BARNES, G. R., BROOKES, M. J. & BOWTELL, R. 2018. A bi-planar coil system for nulling background magnetic fields in scalp mounted magnetoencephalography. *NeuroImage,* 181**,** 760-774.

HOLMES, N., TIERNEY, T. M., LEGGETT, J., BOTO, E., MELLOR, S., ROBERTS, G., HILL, R. M., SHAH, V., BARNES, G. R. & BROOKES, M. J. 2019. Balanced, bi-planar magnetic field and field gradient coils for field compensation in wearable magnetoencephalography. *Scientific reports,* 9**,** 1-15.

HOSHI, Y. & TAMURA, M. 1993. Detection of dynamic changes in cerebral oxygenation coupled to neuronal function during mental work in man. *Neuroscience letters,* 150**,** 5-8.

HUANG, M.-X., NICHOLS, S., BAKER, D. G., ROBB, A., ANGELES, A., YURGIL, K. A., DRAKE, A., LEVY, M., SONG, T. & MCLAY, R. 2014. Single-subject-based whole-brain MEG slow-wave imaging approach for detecting abnormality in patients with mild traumatic brain injury. *NeuroImage: Clinical,* 5**,** 109-119.

IIVANAINEN, J., STENROOS, M. & PARKKONEN, L. 2017. Measuring MEG closer to the brain: Performance of on-scalp sensor arrays. *NeuroImage,* 147**,** 542-553.

IIVANAINEN, J., ZETTER, R., GRÖN, M., HAKKARAINEN, K. & PARKKONEN, L. 2019. On-scalp MEG system utilizing an actively shielded array of optically-pumped magnetometers. *Neuroimage,* 194**,** 244-258.

IIVANAINEN, J., ZETTER, R. & PARKKONEN, L. 2020. Potential of on-scalp MEG: Robust detection of human visual gamma-band responses. *Human brain mapping,* 41**,** 150-161.

JIANG, X., BIAN, G.-B. & TIAN, Z. 2019. Removal of artifacts from EEG signals: a review. *Sensors,* 19**,** 987.

JOSEPHSON, B. D. 1962. Possible new effects in superconductive tunnelling. *Physics Letters,* 1**,** 251.

JOSEPHSON, B. D. 1974. The discovery of tunnelling supercurrents. *Reviews of Modern Physics,* 46**,** 251-254.

KELLY, H. 1946. Degaussing. Nature Publishing Group.

LEE, Y., KWON, H., YU, K., KIM, J., LEE, S., KIM, M. & KIM, K. 2017. Low-noise magnetoencephalography system cooled by a continuously operating reliquefier. *Superconductor Science and Technology,* 30**,** 084003.

LIN, C. H., TIERNEY, T. M., HOLMES, N., BOTO, E., LEGGETT, J., BESTMANN, S., BOWTELL, R., BROOKES, M. J., BARNES, G. R. & MIALL, R. C. 2019. Using optically pumped magnetometers to measure magnetoencephalographic signals in the human cerebellum. *The Journal of physiology,* 597**,** 4309-4324.

MESSARITAKI, E., KOELEWIJN, L., DIMA, D. C., WILLIAMS, G. M., PERRY, G. & SINGH, K. D. 2017. Assessment and elimination of the effects of head movement on MEG resting-state measures of oscillatory brain activity. *NeuroImage,* 159**,** 302-324.

MEYER, S. S., BONAIUTO, J., LIM, M., ROSSITER, H., WATERS, S., BRADBURY, D., BESTMANN, S., BROOKES, M., CALLAGHAN, M. F., WEISKOPF, N. & BARNES, G. R. 2017. Flexible head-casts for high spatial precision MEG. *Journal of Neuroscience Methods,* 276**,** 38-45.

MUTHUKUMARASWAMY, S. D. 2013. High-frequency brain activity and muscle artifacts in MEG/EEG: a review and recommendations. *Front Hum Neurosci,* 7**,** 138.

NARDELLI, N., PERRY, A., KRZYZEWSKI, S. & KNAPPE, S. 2020. A conformal array of microfabricated optically-pumped first-order gradiometers for magnetoencephalography. *EPJ Quantum Technology,* 7**,** 11.

NURMINEN, J., TAULU, S., NENONEN, J., HELLE, L., SIMOLA, J. & AHONEN, A. 2013. Improving MEG performance with additional tangential sensors. *IEEE Transactions on Biomedical Engineering,* 60**,** 2559-2566.

OGAWA, S., LEE, T. M., NAYAK, A. S. & GLYNN, P. 1990. Oxygenation-sensitive contrast in magnetic resonance image of rodent brain at high magnetic fields. *Magnetic resonance in medicine,* 14**,** 68-78.

ÖISJÖEN, F., SCHNEIDERMAN, J. F., FIGUERAS, G. A., CHUKHARKIN, M. L., KALABUKHOV, A., HEDSTRÖM, A., ELAM, M. & WINKLER, D. 2012. High-Tc superconducting quantum interference device recordings of spontaneous brain activity: Towards high-Tc magnetoencephalography. *Applied Physics Letters,* 100**,** 132601.

OKADA, Y., HÄMÄLÄINEN, M., PRATT, K., MASCARENAS, A., MILLER, P., HAN, M., ROBLES, J., CAVALLINI, A., POWER, B., SIENG, K., SUN, L., LEW, S., DOSHI, C., AHTAM, B., DINH, C., ESCH, L., GRANT, E., NUMMENMAA, A. & PAULSON, D. 2016. BabyMEG: A whole-head pediatric magnetoencephalography system for human brain development research. *Rev Sci Instrum,* 87**,** 094301.

OSBORNE, J., ORTON, J., ALEM, O. & SHAH, V. Fully integrated standalone zero field optically pumped magnetometer for biomagnetism. Steep Dispersion Engineering and Opto-Atomic Precision Metrology XI, 2018. International Society for Optics and Photonics, 105481G.

PRATT, E. J., LEDBETTER, M., JIMÉNEZ-MARTÍNEZ, R., SHAPIRO, B., SOLON, A., IWATA, G. Z., GARBER, S., GORMLEY, J., DECKER, D. & DELGADILLO, D. Kernel Flux: a whole-head 432-magnetometer optically-pumped magnetoencephalography (OP-MEG) system for brain activity imaging during natural human experiences. Optical and Quantum Sensing and Precision Metrology, 2021. International Society for Optics and Photonics, 1170032.

ROBERTS, G., HOLMES, N., ALEXANDER, N., BOTO, E., LEGGETT, J., HILL, R. M., SHAH, V., REA, M., VAUGHAN, R. & MAGUIRE, E. A. 2019a. Towards OPM-MEG in a virtual reality environment. *NeuroImage,* 199**,** 408-417.

ROBERTS, T. P., MATSUZAKI, J., BLASKEY, L., BLOY, L., EDGAR, J. C., KIM, M., KU, M., KUSCHNER, E. S. & EMBICK, D. 2019b. Delayed M50/M100 evoked response component latency in minimally verbal/nonverbal children who have autism spectrum disorder. *Molecular autism,* 10**,** 1-10.

RONDIN, L., TETIENNE, J. P., HINGANT, T., ROCH, J. F., MALETINSKY, P. & JACQUES, V. 2014. Magnetometry with nitrogen-vacancy defects in diamond. *Reports on Progress in Physics,* 77**,** 056503.

SANDER, T., PREUSSER, J., MHASKAR, R., KITCHING, J., TRAHMS, L. & KNAPPE, S. 2012. Magnetoencephalography with a chip-scale atomic magnetometer. *Biomedical optics express,* 3**,** 981-990.

SHAH, V. & ROMALIS, M. 2009. Spin-exchange relaxation-free magnetometry using elliptically polarized light. *Physical Review A,* 80**,** 013416.

SHAH, V. K. & WAKAI, R. T. 2013. A compact, high performance atomic magnetometer for biomedical applications. *Physics in Medicine & Biology,* 58**,** 8153.

SILVER, A. & ZIMMERMAN, J. 1965. Quantum transitions and loss in multiply connected superconductors. *Physical Review Letters,* 15**,** 888.

TIERNEY, T. M., LEVY, A., BARRY, D. N., MEYER, S. S., SHIGIHARA, Y., EVERATT, M., MELLOR, S., LOPEZ, J. D., BESTMANN, S. & HOLMES, N. 2021. Mouth magnetoencephalography: A unique perspective on the human hippocampus. *NeuroImage,* 225**,** 117443.

TROEBINGER, L., LÓPEZ, J. D., LUTTI, A., BRADBURY, D., BESTMANN, S. & BARNES, G. 2014. High precision anatomy for MEG. *Neuroimage,* 86**,** 583-591.

TROMP, J., PEETERS, D., MEYER, A. S. & HAGOORT, P. 2018. The combined use of virtual reality and EEG to study language processing in naturalistic environments. *Behavior Research Methods,* 50**,** 862-869.

VIVEKANANDA, U., MELLOR, S., TIERNEY, T. M., HOLMES, N., BOTO, E., LEGGETT, J., ROBERTS, G., HILL, R. M., LITVAK, V. & BROOKES, M. J. 2020. Optically pumped magnetoencephalography in epilepsy. *Annals of clinical and translational neurology,* 7**,** 397-401.

ZETTER, R., IIVANAINEN, J. & PARKKONEN, L. 2019. Optical Co-registration of MRI and On-scalp MEG. *Scientific Reports,* 9**,** 5490.